TSINGHUA SCIENCE AND TECHNOLOGY
ISSN 1007-0214 04/20 pp25-29
Volume 15, Number 1, February 2010

Quality Evaluation of Image Recording Strategies for Limited Angle Tomography*

Fabian Stopp[1,**], Christian Winne[2], Emanuel Jank[2], Erwin Keeve[1,2]

1. Department of Maxillofacial Surgery and Clinical Navigation, Charité – Universitätsmedizin Berlin, 13353 Berlin, Germany;
2. Fraunhofer Institute for Production Systems and Design Technology, 10587 Berlin, Germany

Abstract: In this paper we propose a new method for evaluating image recording strategies for limited angle tomography. In limited angle tomography exact three-dimensional (3-D) reconstruction is not achievable. With this method a metric for the reachable reconstruction quality by defined X-ray source trajectories is calculated. The result of our method is independent of reconstruction algorithms. Our approach is based on the gradients of the scanned volume and their grade of determinability. Compared to simulated reconstruction accuracy with simultaneous algebraic reconstruction techniques, the method of evaluation shows the same dependencies on X-ray source trajectories. By using the proposed method different source trajectories for a limited angle range are comparable with respect to the reachable reconstruction quality.

Key words: 3-D reconstruction quality; intraoperative imaging; limited angle tomography; X-ray source trajectories

Introduction

Commercial three-dimensional (3-D) imaging systems, like 3-D C-Arms and computed tomographys (CTs), are characterized by a circular movement of the X-ray source and the image detector. With this design specific demands on intraopertive use of 3-D imaging are not optimally fulfilled, like unobstructed access to the patient, short imaging time, and low radiation exposure. To improve the usability of intraoperative 3-D imaging, the development of a new imaging concept is required[1]. Alternative X-ray source trajectories have already been presented, e.g., a closed sinusoid trajectory[2] and a wobble trajectory[3] for 3-D C-Arm imaging. To evaluate the reconstruction quality of X-ray source trajectories, computer generated phantoms and reconstruction algorithms are used to calculate the resulting accuracies[4]. An alternative method is presented in Ref. [5]. A resolution function is suggested to predict the tomographic capability of image recording strategies respective to single features in the scanned volume. The features are assessed in reconstruction accuracy independent of reconstruction algorithms. An estimation of the total reconstruction quality of an image recording strategy is not described. A visual method for evaluating X-ray source trajectories is shown in Ref. [6]. Surfaces depending on the trajectory are drawn within a sphere representing the reconstruction volume. The source trajectory is complete if the surfaces fill the sphere sufficiently.

The condition for a complete trajectory and exact reconstruction respectively is described by Tuy[7]. For an exact reconstruction of a point this condition requires that every plane passing through the point has to intersect the X-ray source trajectory at least once. X-ray source trajectories of limited angle tomographies do not fulfil Tuy's condition (Fig. 1).

Received: 2009-10-19
* Supported by the German Federal Ministry of Education and Research (No. 01EZ0839)
** To whom correspondence should be addressed.
E-mail: fabian.stopp@charite.de

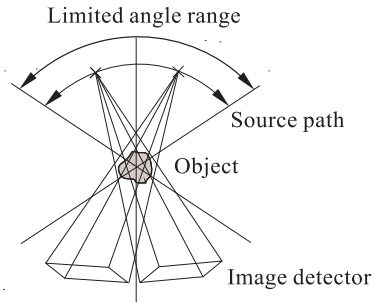

Fig. 1 Example of limited angle tomography

The 3-D reconstruction result of a vertebral body is shown in Fig. 2. 48 projection images of the body were acquired by a circular X-ray source and image trajectory. In Fig. 2a the angle range of the trajectory is 180° and in Fig. 2b 120°. The limited angle range of Fig. 2b leads to artifacts in the 3-D reconstructed volume, visible at the borders of the spinal canal.

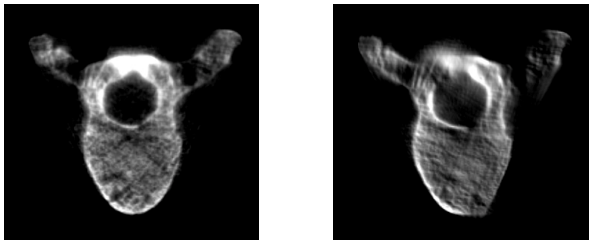

(a) 180° (b) 120°

Fig. 2 Axial slices of a 3-D reconstructed vertebral body with a circular source and image trajectory and 48 projection images; the angle range of the circular trajectory is (a) 180° and (b) 120°.

The reconstruction quality of limited angle tomographies is difficult to predict. The evaluation of X-ray source trajectories by comparing reconstructed volumes is time-consuming, depends on used reconstruction algorithms and is not usable for mathematical optimization of source trajectories. Therefore a metric describing the reachable reconstruction quality is necessary.

In this article a new method for evaluating X-ray source trajectories for limited angle tomography is proposed. The method describes the reconstruction quality of a volume element based on a defined X-ray source trajectory. Our quality evaluation is independent of reconstruction algorithms and any point in the scanned volume can be considered. The scanned volume is assumed to be completely pictured in the projection images. With this method different image recording strategies within a limited angle range are comparable in resulting 3-D reconstruction quality.

1 Quality Evaluation Method

Our approach is based on the determinability of the gradients at one point in the volume. The gradients describe the density changes in defined directions inside the volume. It can be observed that a gradient $\boldsymbol{\theta}$ at a point $\boldsymbol{p}$ in the direction of the X-ray beam from source position $\boldsymbol{s}$ is not displayed in the projection image of the beam. With growing difference between direction of gradient and X-ray beam, the changes of the density are better visible in the images. The projection of the gradients in the images depends on the angle φ between the gradients and the X-ray beam.

Only information contained in the projection images can be reconstructed. Because density changes in direction of the X-ray beam are not visible in the images, the reconstruction accuracy of a point depends on the projection of the gradients at this point. Because the X-ray source $\boldsymbol{s}$, the X-ray beam, the point $\boldsymbol{p}$ in the volume, and the gradient $\boldsymbol{\theta}$ are located in a plane, the two-dimensional space is considered.

With the Radon transform the projection of a density function $f(x,y)$ can be described with line integrals of this function (Fig. 3). The (ξ,η)-coordinate system rotates with the X-ray source $\boldsymbol{s}$. The (x,y)-coordinate system of the density function and the (ξ,η)-coordinate system have the following geometrical relation:

$$x=-\xi\sin\varphi+\eta\cos\varphi \tag{1}$$

$$y=\xi\cos\varphi+\eta\sin\varphi \tag{2}$$

For a constant angle of projection φ the projection integral for parallel beam geometry is

$$p_{\varphi}(\xi)=\int_{-\infty}^{\infty} f(\xi\boldsymbol{n}_{\xi}+\eta\boldsymbol{n}_{\eta})\mathrm{d}\eta \tag{3}$$

The vectors $\boldsymbol{n}_{\xi}$ and $\boldsymbol{n}_{\eta}$ are the unit vectors in direction of the lateral shift of the X-ray source as well as

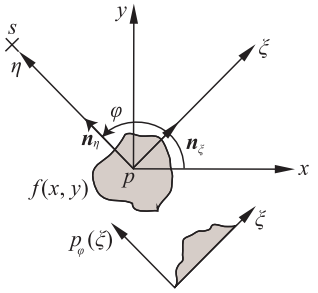

Fig. 3 Line scanning of density function *f*

in direction of projection.

$$\boldsymbol{n}_\xi = (-\sin\varphi, \cos\varphi)^{\mathrm{T}};\ \boldsymbol{n}_\eta = (\cos\varphi, \sin\varphi)^{\mathrm{T}} \quad (4)$$

In order to determine the gradient projection of the density function f at point $\boldsymbol{p}$, Eq. (3) is differentiated with respect to ξ.

$$\frac{\partial}{\partial\xi} p_\varphi(\xi) = \frac{\partial}{\partial\xi} \int_{-\infty}^{\infty} f\left(\xi\begin{pmatrix}-\sin\varphi\\ \cos\varphi\end{pmatrix} + \eta\begin{pmatrix}\cos\varphi\\ \sin\varphi\end{pmatrix}\right) \mathrm{d}\eta \quad (5)$$

Using Eqs. (1) and (2), we can transform the derivative Eq. (5) to:

$$\frac{\partial}{\partial\xi} p_\varphi(\xi) = \int_{-\infty}^{\infty} \left(\begin{pmatrix}\frac{\partial}{\partial x} f & \frac{\partial}{\partial y} f\end{pmatrix}\begin{pmatrix}-\sin\varphi\\ \cos\varphi\end{pmatrix}\right) \mathrm{d}\eta \quad (6)$$

$$\frac{\partial}{\partial\xi} p_\varphi(\xi) = -\sin\varphi \int_{-\infty}^{\infty} \frac{\partial}{\partial x} f(\xi\boldsymbol{n}_\xi + \eta\boldsymbol{n}_\eta)\mathrm{d}\eta + \cos\varphi \int_{-\infty}^{\infty} \frac{\partial}{\partial y} f(\xi\boldsymbol{n}_\xi + \eta\boldsymbol{n}_\eta)\mathrm{d}\eta \quad (7)$$

If the x-axis of the (x, y)-coordinate system is interpreted as the direction of the gradient $\boldsymbol{\theta}$, the gradient $\partial f/\partial x$ is multiplied by $\sin\varphi$ in the differentiation of the Radon transform. An equivalent proof of this observation can also be shown for fan-beam geometry.

A quality function q is defined, where the gradient $\boldsymbol{\theta}$ is weighted with the sine of the angle φ between the X-ray beam and the gradient direction.

$$q(\boldsymbol{p}, \boldsymbol{s}, \boldsymbol{\theta}) = \sin\varphi = \sin\left(\left|\arccos\left(\boldsymbol{\theta} \cdot \frac{\boldsymbol{p}-\boldsymbol{s}}{\|\boldsymbol{p}-\boldsymbol{s}\|}\right)\right|\right),$$

$$q : \mathbb{R}^3 \times \mathbb{R}^3 \times S^2 \to [0,1], \text{with } S^2 = \{\boldsymbol{x} \in \mathbb{R}^3 : \|\boldsymbol{x}\| = 1\} \quad (8)$$

For a set of projections from different directions to point $\boldsymbol{p}$ each gradient is weighted with the maximal quality value of all N_S X-ray source positions.

$$q(\boldsymbol{p}, \boldsymbol{\theta}) = \max(q(\boldsymbol{p}, \boldsymbol{s}_i, \boldsymbol{\theta}) | i \in \{1, 2, ..., N_\mathrm{S}\}) \quad (9)$$

With a set of X-ray source positions the value $q(\boldsymbol{p}, \boldsymbol{\theta})$ of the quality function for a gradient direction describes an upper bound of the determinability.

The quality function $q(\boldsymbol{p}, \boldsymbol{\theta}_j)$ is calculated for all gradient directions $\boldsymbol{\theta}_j, j \in 1, \ldots, N_\mathrm{g}$ emanating from point $\boldsymbol{p}$. The result of q is 0 for same directions of $\boldsymbol{\theta}$ and X-ray beam and 1 if they are orthogonal. With a unit sphere considering the point $\boldsymbol{p}$ in the center of the sphere the results of q can be visualized. At the intersection points of the gradients $\boldsymbol{\theta}_j$ with the surface of the unit sphere the quality values of the respective gradient directions are illustrated. In Fig. 4 the gradient unit sphere is shown for $N_\mathrm{S} = 20$ X-ray source positions on a circular 120° trajectory.

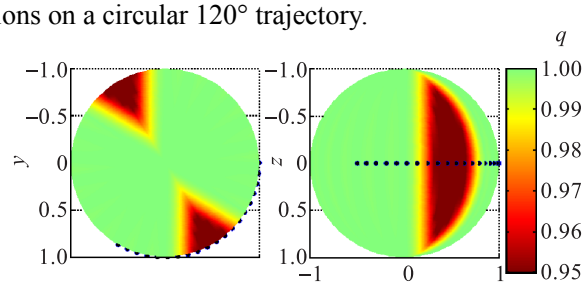

Fig. 4 Quality visualization with a gradient unit sphere for 20 X-ray source positions on a 120° circular trajectory. The points represent the source positions, the surface of the sphere shows the quality $q(\boldsymbol{p}, \boldsymbol{\theta}_j)$ of the gradients $\boldsymbol{\theta}_j$ emanating from sphere center $\boldsymbol{p}=(0,0,0)^{\mathrm{T}}$ in all directions.

To determine the quality of the reconstruction at position $\boldsymbol{p}$, the mean quality value $q(\boldsymbol{p})$ of all gradients $\boldsymbol{\theta} \in S^2$ is calculated.

$$q(\boldsymbol{p}) = \frac{1}{\pi}\int_0^{\pi} \frac{1}{2\pi}\int_0^{2\pi} q(\boldsymbol{p}, \boldsymbol{\theta}(\phi, \vartheta))\mathrm{d}\phi\mathrm{d}\vartheta \quad (10)$$

$$\text{with } \boldsymbol{\theta}(\phi, \vartheta) = (\sin\vartheta\cos\phi, \sin\vartheta\sin\phi, \cos\vartheta)^{\mathrm{T}} \quad (11)$$

2 Comparison with Simulated SART Reconstruction Accuracy

To evaluate our proposed method of gradient determinability we compared it to accuracy determination with simultaneous algebraic reconstruction technique (SART)[8]. The SART is used because of the analysis of our method with limited angle source trajectories and a limited number of projection images.

2.1 X-ray source trajectories

Three different classes of X-ray source trajectories for 3-D reconstruction are defined. Every class consists of a trajectory with a variable parameter. By a modification of the variable parameter the source trajectory is changed and influenced in resulting reconstruction quality (see Fig. 5).

The circular path (Fig. 5 left) is an X-ray source trajectory around the volume with a variable angle at center ϕ_c. The angle at the center varies from 90° to 180° in 15°-steps.

The crosswise path with central intersection (Fig. 5 middle) is a source trajectory consisting of two single circular paths around the volume. The circuits intersect orthogonally in their center. The angle at center of the first circuit ϕ_c is 90° and the angle at the center of the

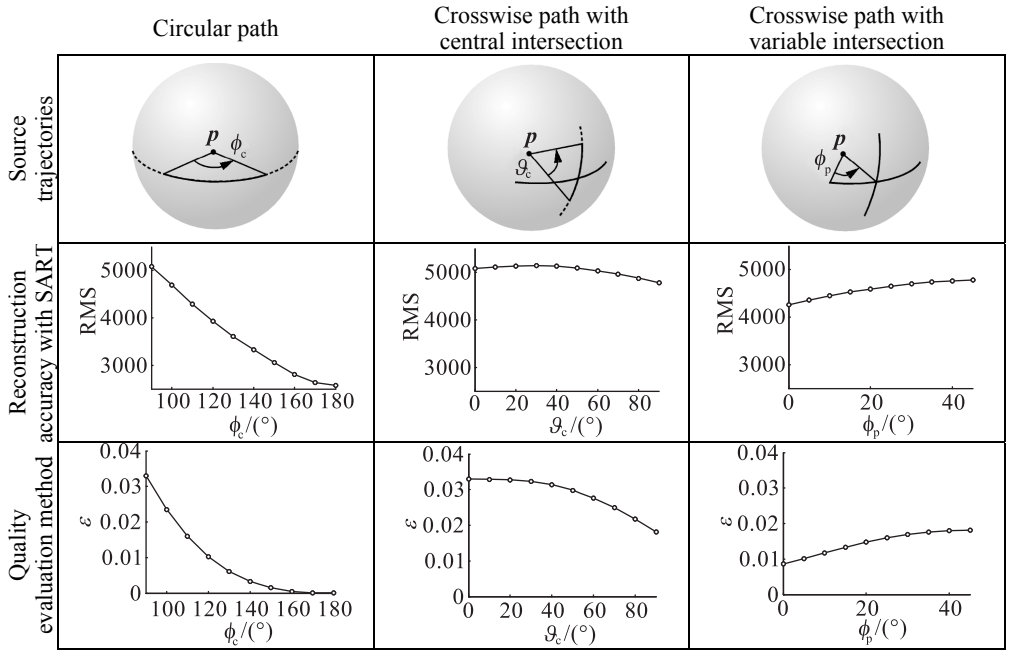

Fig. 5 Comparison with SART reconstruction accuracy: row 1: defined X-ray source trajectories with variable parameters ϕ_c, ϑ_c, and ϕ_p; row 2: accuracies of SART reconstructions; row 3: results of our proposed quality evaluation method.

second circuit ϑ_c varies from 0° to 90° in 10°-steps.

The crosswise path with variable intersection (Fig. 5 right) is a source trajectory consisting of two single circular paths around the volume. The angles at center ϕ_c and ϑ_c of these two circuits are constant with 90°. The circuits intersect orthogonally in the center of the second path. The angle position ϕ_p of the point of intersection on the first circuit is variable. The angle ϕ_p varies from 0° to 45° in 5°-steps.

2.2 Quality evaluation with SART

With a software environment two-dimensional projection images of the Shepp-Logan phantom[9] were produced based on the three defined types of source trajectories. For each source trajectory 180 cone-beam projection images were created. All 180 source positions were evenly distributed over the complete possible path. The Shepp-Logan phantom was located in the center of the circular paths. The distance between X-ray source and center of the phantom was 20 mm. The distance from X-ray source to the detector was 40 mm. The central beam of the X-ray source formed the normal of the image plane. The size of the image was 5.5 mm×5.5 mm with 1024×1024 pixels. The reconstructed volume consisted of 256×256×256 voxels with a voxel size of 0.01 mm^3. The reconstruction algorithm used was SART with three iterations. The results of the reconstructed volumes V were compared with the original phantom P. The range of the density values of V and P was between 0 and 65 535. To determine the resulting accuracy the difference between original and reconstruction is calculated for each voxel of the volume. With the normalized root mean square (RMS) of all differences the reconstruction quality is specified.

$$\mathrm{RMS}=\sqrt{\frac{1}{256^3}\sum_{x=1}^{256}\sum_{y=1}^{256}\sum_{z=1}^{256}(V_{x,y,z}-P_{x,y,z})^2} \qquad (12)$$

2.3 Quality evaluation with our method

The arrangement of source positions and volume was exactly the same as in the quality evaluation with SART. To compensate the different dimensions of Shepp-Logan phantom and gradient unit sphere, the size of the whole configuration was scaled with factor 20. For each recording strategy 180 source positions were used. The volume in the center of the unit sphere was the same proportion of size compared to the simulation with SART and consisted of 3×3×3 points. The considered $N_g=10\,000$ gradients at each of these points were uniformly distributed in all directions. Every gradient of the $N_p=27$ volume points was determined with the maximal quality value of all projections (Eq. (9)).

As the total quality measurement of one complete source trajectory the arithmetic mean μ and the error value ε of all gradient quality values are calculated:

$$\varepsilon = 1 - \mu \quad \text{with} \quad \mu = \frac{1}{N_\mathrm{p} \cdot N_\mathrm{g}} \sum_{i=1}^{N_\mathrm{p}} \sum_{j=1}^{N_\mathrm{g}} q(\boldsymbol{p}, \boldsymbol{\theta}_{i,j}) \quad (13)$$

3 Results

The results of our method were compared with the results calculated with SART. The error values of our method have similar dependencies on the X-ray source trajectory as the results of SART. This is shown for all defined recording strategies depending on their respective parameters. The graphical presentation of the comparison is illustrated in Fig. 5.

With increasing angle ϕ_c of the circular path the error values ε and RMS decreased. The slopes of both error curves also decreased with a growing angle ϕ_c (Fig. 5 left). The most accurate results were achieved with an angle $\phi_\mathrm{c} = 180°$. For the central point in the scanned volume this trajectory fulfilled the sufficiency condition. The RMS error was 2580 for a total density range from 0 to 65 535. The RMS value was caused by the comparison of the reconstructed volume with the discretized mathematic defined Shepp-Logan phantom. This led to increased differences at the density borders of the discretized phantom and the slightly blurred reconstruction. For the crosswise path with variable intersection the error values ε and RMS showed the same variation depending on a change of ϕ_p (Fig. 5 right). By changing the intersection of both circuits from $\phi_\mathrm{p} = 0°$ to $\phi_\mathrm{p} = 45°$ the reconstruction accuracy decreased continuously.

In contrast to our method the SART reconstruction error rose with increasing angle ϑ_c from 0° to 30° (Fig. 5 middle). Because of the constant number of 180 source positions, the distances between the positions on the first circuit grew with an increasing angle ϑ_c. The increasing density of source positions near the central intersection decreased the weighting of projections from outer positions in calculating the reconstruction with SART. With an angle ϑ_c greater than 30° the error values ε and RMS showed again the same dependency on ϑ_c.

4 Conclusions

In this paper a method for evaluating image recording strategies for limited angle tomography is proposed. This method computes a metric for the reachable reconstruction quality of any considered point in the scanned volume. The result of the method depends on the X-ray source positions in relation to the considered point in the volume and is independent of reconstruction algorithms. Compared to simulated reconstruction accuracy with SART, our quality evaluation method shows the same dependencies on X-ray source trajectories. The method can be used to compare the reachable 3-D reconstruction quality of different image recording strategies. In future work we use the proposed method to determine optimal image recording strategies for limited angle tomography. Using mathematical optimization methods, we calculate the optimal arrangement of X-ray source positions within a predefined limited angle range, regarding the 3-D reconstruction quality and radiation exposure.

References

[1] Jank E. Assumption for improving intraoperative 3D X-ray scanners. *International Journal of Computer Assisted Radiology and Surgery*, 2008, **S1**: 347.

[2] Yang H, Li M, Koizumi K, et al. Closed sinusoid trajectory for C-arm CT imaging. In: Proceedings of IEEE Nuclear Science Symposium Conference. San Diego, USA, 2006, **M14-456**: 3480-3484.

[3] Tita R, Lüth T C. Free isocentric 3d imaging and a novel approach for wobble trajectories using a modified standard c-arm. In: Proceedings of IEEE Engineering in Medicine and Biology Society. Lyon, France, 2007: 4418-4421.

[4] Ramamurthi K, Prince J L, Strobel N. Exact 3d cone-beam reconstruction from projections obtained over a wobble trajectory on a c-arm. In: Proceedings of IEEE International Symposium on Biomedical Imaging. Arlington, USA, 2004, **1**: 932-935.

[5] Clackdoyle R, Noo F. Cone-beam tomography from 12 pinhole vertices. In: Proceedings of IEEE Nuclear Science Symposium Conference. San Diego, USA, 2001, **4**: 1874-1876.

[6] Schomberg H. Complete source trajectories for C-arm systems and a method for coping with truncated cone-beam projections. In: Proceedings of the 6th International Meeting on Fully Three-Dimensional Image Reconstruction in Radiology and Nuclear Medicine. Asilomar, CA, 2001.

[7] Tuy H K. An inversion formula for cone-beam reconstruction. *SIAM Journal on Applied Mathematics*, 1983, **43**: 546-552.

[8] Andersen A H, Kak A C. Simultaneous algebraic reconstruction technique (SART): A superior implementation of the art algorithm. *Ultrasonic Imaging*, 1984, **6**(1): 81-94.

[9] Yu H, Ye Y, Wang G. Katsevich-type algorithms for variable radius spiral cone-beam CT. In: Proceedings of SPIE. 2004, **5535**: 550-557.